Applied Surface Science 287 (2013) 37–45

Applied Surface Science

journal homepage: www.elsevier.com/locate/apsusc

Surface charges of oxides and wettability: Application to TiO_2–SiO_2 composite films

J.-C. Joud*, M. Houmard[1], G. Berthomé

SIMaP-Grenoble Institute of Technology, BP 75, 38402 Saint Martin d'Hères, France

ARTICLE INFO

Article history:
Received 8 July 2013
Received in revised form 30 August 2013
Accepted 9 September 2013
Available online 17 September 2013

Keywords:
Surface charge and wettability
Super-hydrophilicity
TiO_2–SiO_2 thin films
Prewetting film
Resistance to vaporization

ABSTRACT

The super-hydrophilicity which can exist at the interface between oxides and aqueous solutions is able to sustain industrial and domestic applications. Several experimental results obtained on TiO_2–SiO_2 composite thin films via a sol–gel route have confirmed a natural and persistent super hydrophilicity under standard atmosphere. This property can be easily photo-regenerated after a long aging period in ambient atmosphere using a short UV illumination. The electrochemical double layer which classically exists between oxide surfaces and aqueous solution is unfavorable to high wettability properties of ideal flat surfaces. The present study indicates how the surface rugosity and the disjoining pressure caused by surface charges are able to explain the stability of a prewetting film. This film can withstand to vaporization in a weakly under saturated atmosphere, having a protective action despite a carbon contamination brought by standard atmosphere.

1. Introduction

Wetting phenomena are essential in a variety of natural and technological processes. Wetting of solids has been extensively studied from the theoretical and experimental point of view during the past two decades [1–5,8].

The super hydrophobicity phenomenon, revealed recently on a variety of natural and artificial objects is responsible of growing interest [4,6–8]. The interest being the minimization of interactions between the liquid and the substrate.

The present paper deals with the opposite situation where the solid exhibits a high hydrophilicity with an apparent contact angle of water droplet close to 0°.

This case is interesting for the cleaning of a surface contaminated by oily substances that we have studied on stainless steel substrates covered by such composite films [9,10].

During the last years we have studied the wettability properties of various types of composite films obtained using a sol–gel route. These films which are made by mixing oxides (TiO_2–SiO_2) exhibit high wettability characterized by water contact angles ranging between 0° and 5°. In addition these results maintain stable over a significant period of time (7–8 weeks) under exposition to standard laboratory atmosphere.

The interface between solid oxides and water exhibits an electrochemical double layer which generally prevents high wettability properties [2]. So the aim of this paper is to develop a theoretical analysis in order to explain our experimental results and particularly to understand the stable high wettability observed under standard atmosphere.

The present paper is divided in three parts. The first one recall briefly the main experimental results obtained in previous publications focusing on wettability experiments and surface charges determinations. This part is completed by new experimental results presented in the PhD thesis of Dr Houmard [16]. The second part of our paper is dedicated to a physico-chemical analysis taking into account the presence of an electrochemical double layer which exists at the interface between the oxide and the liquid solution. The stability of the prewetting film which exists in front of the contact line is able to explain the capacity of the liquid film to withstand to vaporization in a weakly dry atmosphere. Based on this analysis, the formation and the stability of prewetting film are discussed in a third part. Theoretical results indicate the possible existence of a prewetting film in a weakly under-saturated atmosphere in agreement with the experimental observations. Then a short conclusion is proposed.

2. Super hydrophilic solid: experimental results

In the following we present selected issues of the experimental results obtained in our Lab which have been published in

* Corresponding author. Tel.: +33 476826507.
E-mail address: Jean-Charles.Joud@grenoble-inp.fr (J.-C. Joud).
[1] Present address: Universidade Federal de Minas Gerais-Escola de Engenharia, 1-3304, Belo Horizonte, MG 31270-901, Brazil.

0169-4332
http://dx.doi.org/10.1016/j.apsusc.2013.09.054

Table 1
Surface morphology of S4 composite films with indications of RMS roughness and mean values of pore radii r_p and interconnected necks radii r_n.

Film nomenclature	Mean pore radii r_p/r_n (nm)	RMS roughness (nm)
S4-20	5.0/3.7	8.8
S4-40	7.5/5	9.2
S4-60	Limit of the detection range	10.9

various papers [9–13]. These experimental results summarize and characterize the surface properties we have to explain by a new theoretical analysis including the existence of an electrochemical double layer.

2.1. Preparation of TiO_2–SiO_2 solutions and composite films

Titania–silica composite films were deposited from mixtures of a TiO_2 anatase crystalline suspension and polymeric SiO_2 solutions. A polymeric mother solution (MS) was first prepared by tetraisopropyl orthotitanate (TIPT) with deionised water, hydrochloric acid and pure ethanol as solvent.

Then a crystalline suspension (CS) of TiO_2 nanocrystallites in absolute ethanol was prepared from the MS using a multi-step procedure that has been previously detailed [11] including autoclaving at 130 °C for 6 h. The final procedure is performed in order to remove water from the sol and form a CS in absolute ethanol with final TiO_2 concentration of 0.24 M. The CS was composed of TiO_2 nano-particles crystallized in the anatase phase with a diameter of about 5–6 nm [12].

In parallel, polymeric silica sol were elaborated from tetraethoxysilane (TEOS). Various silica sol formulations have been extensively studied in a previous publication [9]. Two silica sol formulations, labeled S2 and S4 are selected as more characteristic. These formulations present a similar TEOS concentration (0.24 mol/L) and different pHs and H_2O/TEOS molar ratios (respectively for S2: 3.5 and 2.2; for S4: 2 and 0.5).

Finally, S2 and S4 sols were mixed with the crystalline suspension in 20, 40, 60, 80 Si/(Si + Ti) molar ratios yielding TiO_2–SiO_2 solutions which were used for composite film deposition. The film deposition was performed on (1 0 0) silicon wafers by spin-coating (300 μL of solution, spin speed of 3000 rpm) at room temperature. Prior to deposition the substrates were simply cleaned with ethanol and then dried with air spray. This easy cleaning procedure is sufficient to produce composite films with a good homogeneity and optical quality. As deposited films were then heat treated for 2 h at 500 °C. The thickness of resulting composite films varied between 30 and 70 nm depending on the formulation of the silica sol.

2.2. Surface characterization of the films

2.2.1. Surface morphology of composite films

The open porosity of the films was studied by an ellipsometric porosimetry at atmospheric pressure using a commercially device (EPA SOPRA), RMS roughness measurements are obtained using an atomic force microscope in tapping mode (AFM, digital instrument nanoscope multimode).

Experimental observations which are presented and discussed in previous papers [9,13] are summarized in Table 1 for the S4 films. In this study the open porosity of the films is assimilated to pores of mean radius r_p interconnected by necks of smaller mean radius r_n.

The RMS roughness deduced from AFM measurements is rather well correlated to the pore size of S4 composite films. In addition we know that the RMS roughness does not depict perfectly the surface morphology features. So the AFM experiments allow calculating the ratio r which is the ratio of the real surface over the projected one. With the AFM acquisition conditions the ratio r is found to be close to 1.2 with a variation of 10% for the S4 composite films.

However the experimental observations (FEG-SEM and AFM images) performed on various samples (S1 and S4 composites) indicate a larger variation of the measured RMS roughness than the calculated ratio r.

2.2.2. Surface composition and surface charges

Surface analysis was performed by X-ray photoelectron spectroscopy (XPS) using an XR3E2 apparatus from Vacuum Generator using a Mg Kα source (1253.6 eV).

The experimental procedure is presented in detail in a previous paper [9]. The main conclusions obtained on S3 composite films, very similar to the S4 films, can be summarized in Fig. 1.

The deconvolution of the Si 2p and Ti 2p spectra are presented for S3-20, S3-40 and S3-60 composite films. The vertical lines indicate respectively the binding energy measured for pure SiO_2 and TiO_2 films. We observe clear and opposite chemical shifts on the main Si^{4+} and Ti^{4+} peaks.

These results suggest the existence of dipole charges at the interfaces between TiO_2 grains and SiO_2 fibers of the samples.

The surface charge characterization has been conducted using a new AFM apparatus in liquid configuration (Autoprobe CP from Park Scientific Instruments CA, USA)

The composite film is immersed in liquid water at a controlled pH (deionized water at pH 5.7).

At the extremity of the cantilever a sphere of pure SiO_2 (Novascan, USA) with a diameter of 20 μm is fixed and interacts with the sample in a standard configuration (sphere/plan). The forces which are developed between the reference sphere and the surface of the sample are analyzed using the classical D.L.V.O. theory [14]. At large distance the electrostatic interactions $F(D)$ dominate the Van der Waals attraction and can be represented by a simple formula [16]. Due to the PZC (point of zero charge) values of TiO_2 and SiO_2 (respectively 6.5 and 2) the electrostatic interactions prevail between the SiO_2 sphere and the SiO_2 component of the composite film allowing the calculation of the surface charges of the sample and the sphere by fitting the experimental $F(D)$ curve with the corresponding theoretical formula [17,18].

$$F_{el.st} = \frac{2\pi\lambda_D R}{\varepsilon\varepsilon_0}\left\{(\sigma_P^2+\sigma_S^2)\exp-\frac{2D}{\lambda_D}+2\sigma_P\sigma_S\ \exp-\frac{D}{\lambda_D}\right\}$$

With: ε, ε_0 the relative and absolute dielectric constant, λ_D the Debye screening length and

σ_P, σ_S the surface charge of the point and substrate.

Approximate values ranging between 2 μC/cm^2 for pure SiO_2 surface and 7 μC/cm^2 for the composite film are obtained.

The experimental results indicated in Fig. 2 clearly confirm the existence of negative surface charges on the S4-60 composite film similar or even larger than that observed on the reference SiO_2 sample with values ranging between 2 and 7 μC/cm^2.

2.3. Contact angles and wettability

Water wettability properties of composite films have been investigated in detail in previous papers [9,10,16]. Fig. 3 summarizes the evolution of the apparent experimental contact angles with aging time in ambient atmosphere for the S2-60 and S4-60 composite films.

As comparison purpose Fig. 4 illustrates the apparent experimental contact angles obtained on pure films (a) TiO_2 and (b) SiO_2.This results have been measured during various periods of time so with slightly different atmospheric atmospheres [16].

It could be stressed that only apparent contact angles can be measured in our experimental investigations.

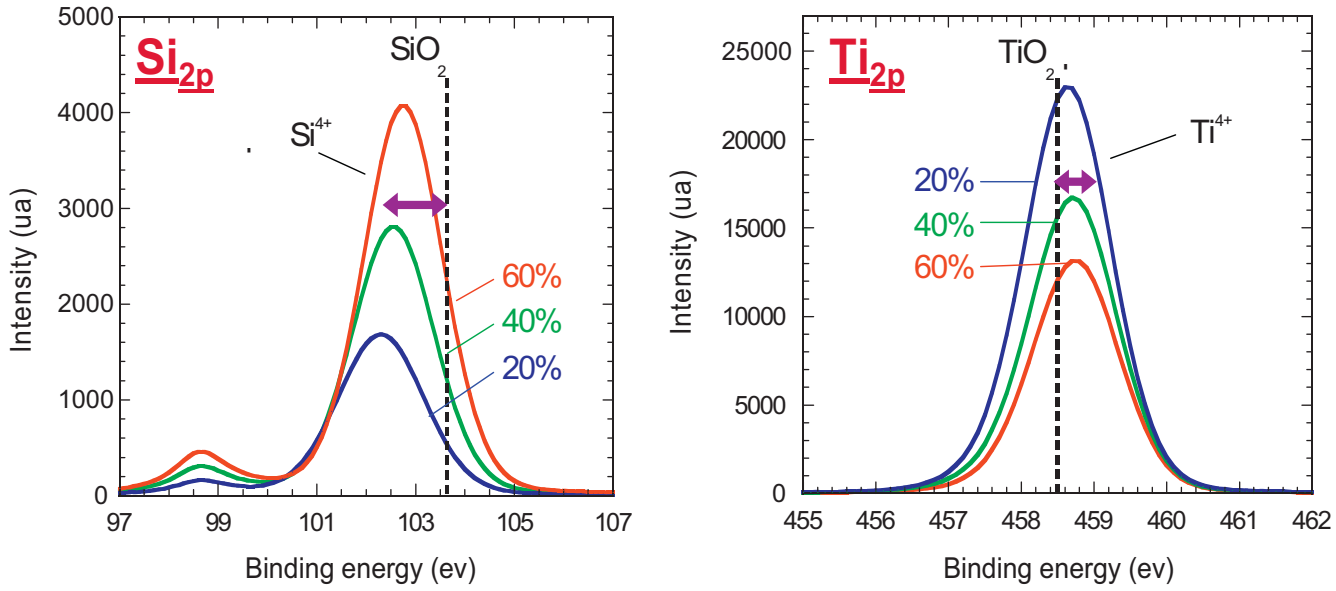

Fig. 1. Spectra of Si 2p and Ti 2p obtained by XPS on composite films S3-20, S3-40 and S3-60. The binding energies of the main Si $^{4+}$ and Ti $^{4+}$ peaks are compared to the reference binding energies of pure SiO_2 and TiO_2 [9].

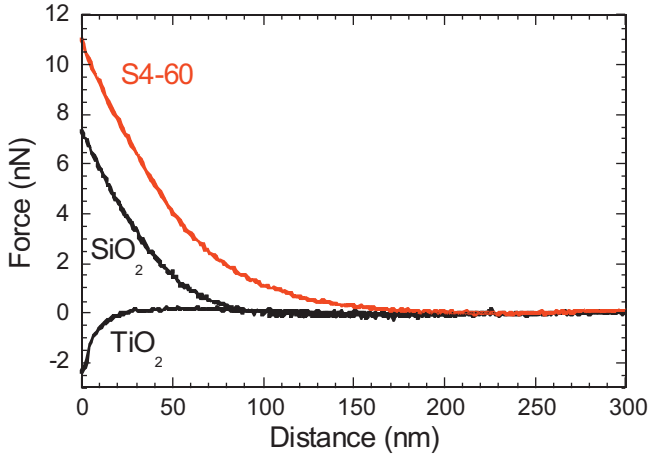

Fig. 2. Curves of forces versus distance between the reference SiO_2 sphere and the surface of the sample in liquid water at pH 5.7. The studied surfaces (pure TiO_2, pure SiO_2 and S4-60) in this AFM experiment have been initially cleaned by an Ar plasma treatment.

Immediately after the thermal treatment at 500 °C of the composite films, the surface exhibits a super hydrophilic character. This character is maintained with aging time for the S4-60 film contrary to the pure SiO_2 sample or pure TiO_2 sample.

We recall that the contact angle figures correspond to averaged values obtained on 5–7 liquid droplets. The relative uncertainty $\Delta\theta/\theta$ varies between 70% for the lowest contact angle around 3–5° and 20% for the highest contact angles closed to 20–25°.

Fig. 5 illustrates the recovery of super hydrophilic properties of the samples after UV illumination. The various films treated in this experiment correspond to samples aged in laboratory atmosphere during 60 days. These curves illustrate the photocatalytic activity of TiO_2 crystallites present in the composite films with a degradation of organic contaminants present at the surface film after aging and a probable surface enrichment with OH groups.

We can notice the disappearance of this effect for the sample with a high SiO_2 content.

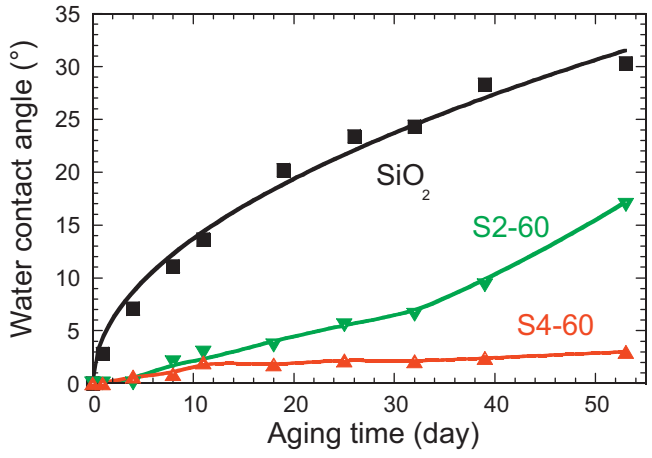

Fig. 3. Evolution of the water contact angles with aging time for the composite films S2-60 and S4-60 comparatively to a pure silica film [9].

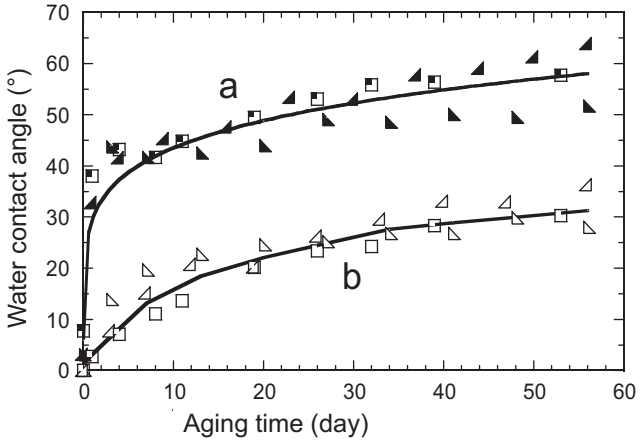

Fig. 4. Evolution of the water contact angle with aging time for (a) pure TiO_2 film and (b) pure SiO_2 film.

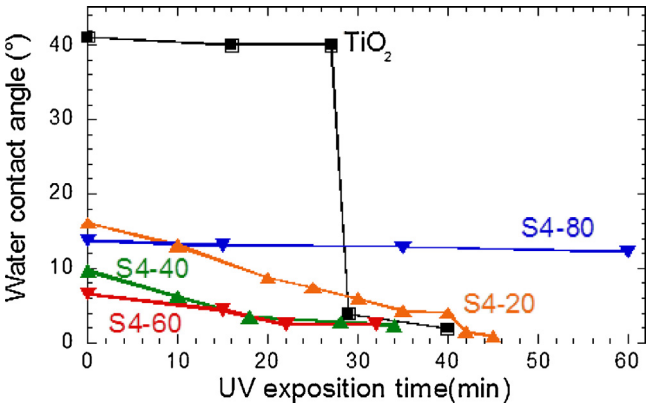

Fig. 5. Recovery of super hydrophilic properties of the samples after UV illumination. The various films treated in this experiment correspond to samples aged in laboratory atmosphere during 60 days [10].

A complementary experiment has been performed on a S4-60 composite film which has been maintained under a vacuum during one week after elaboration. The contact angle measurements are then performed under an Ar atmosphere avoiding any possible condensation of water vapor.

The measured contact angles ranging between 17° and 22° are significantly higher than the standard values measured with a classical protocol (0–5°).This result indicates that the value of the true equilibrium contact angle θ_E in absence of a prewetting film is close to the measured contact angle (17–22°).

Optimization of the S2 and S4 composite films with the silica content of the composite film has been studied in previous papers [9,10,16]. The best hydrophilic property is obtained for the composition SiO_2 = 60%. Better hydrophilic property is obtained for the composite S4-60.

The last experimental result we want to recall deals with enhanced cleanability of such composite films. As detailed in our paper [10] we measure the critical water flow corresponding to the detachment of an oil drop initially laying on a S4-60 composite film aged for 8 weeks in ambient condition. The experiment is done in a ad-hoc flow cell which allows to record the image of the drop shape for increasing laminar flow.

The critical flows are measured for S2 and S4 composite films with respect to the silica content of the film. The best cleanability, which corresponds to the lowest critical flow, is obtained for the S4-60 composite film.

As preliminary conclusions on the experimental results, it can be noticed:

- Surface charges are present at the interface between oxide surfaces and liquid water.
- Very weak contact angles are measured (∼5°) over long exposure time (∼2 months) without UV illumination.

This last point contrast with the classical evolution of the water contact angles measured on pure SiO_2 and TiO_2 oxides over similar period of time. This increase is attributed to a carbon contamination due to the atmosphere as evidenced by XPS experiments [16].

The question to be answered is then, why such a classical contamination has no effect on the composite films.

3. Super hydrophilic solids: theoretical analysis

3.1. Classical situation – basic results

In the case of an hydrophilic solid the solid/liquid contact is favored due to the respective value of solid–liquid and solid–vapor surface tension ($\gamma_{SL} \leq \gamma_{SV}$). Thus the solid–liquid interface is likely to follow the roughness of the solid which leads to an apparent contact angle given by the Wenzel equation [1,4]:

$$\cos\ \theta_{app} = r \cos\ \theta_E \tag{1}$$

With r the roughness of the solid expressed as the ratio of the real surface area over the projected one and θ_E the equilibrium contact angle on a perfect surface corresponding to Young equation

$$\cos\ \theta_E = \frac{\gamma_{SV} - \gamma_{SL}}{\gamma_{LV}} \tag{2}$$

As $\theta_E \leq 90°$ (hydrophilic surface) the apparent contact angle is such that: $\theta_{app} \leq \theta_E$ following the Wenzel equation. Eq. (1) is established using the argument of virtual works with a small displacement of the triple line at equilibrium. This small displacement is done over a dry solid [1,4].

A different phenomenon can occur in the case of a highly hydrophilic case. A highly textured surface can be considered as a two dimensional porous surface on which the liquid can be absorbed.

So the situation can be analyzed using the Cassie Baxter equation [19] which gives the apparent contact angle over a patchwork of solid and liquid phases.

$$\cos\ \theta_{app} = \phi_S \cos\ \theta_E + (1 - \phi_S) \tag{3}$$

with ϕ_S the solid surface fraction and $(1 - \phi_S)$ the liquid surface fraction.

As clearly indicated by de Gennes [1] Eq. (3) is valid if an imbibition film exist in front of the triple line.

This situation corresponds to a "Cassie impregnating state" with water penetrating the pores in the outer vicinity of the droplet as indicated by Bormashenko [22a].

As indicated in Fig. 6 we can evaluate the variation of the free energy of the prewetting film for a progression dx of the front of imbibition assuming a unit width

$$dF = (\gamma_{SL} - \gamma_{SV})(r - \phi_S)dx + \gamma_{LV}(1 - \phi_S)dx \tag{4}$$

The first term expresses the creation of an interface liquid/solid in the inner part of the surface, corrected by the fraction $\phi_S dx$ which corresponds to the external and dry part of the surface. (This point will be discussed in the last part of the paper.) The second term is due to the creation of a liquid/vapor interface. The description of the roughness is over simplified assuming a regular repartition of micro channels at the surface.

The condition of stability of the prewetting film ($dF \leq 0$) with the Young equation gives the following condition:

$$\cos\ \theta_E \geq \frac{1 - \phi_S}{r - \phi_S} = \cos\ \theta^0_{crit} \quad \text{and} \quad \theta_E \leq \theta^0_{crit} \tag{5}$$

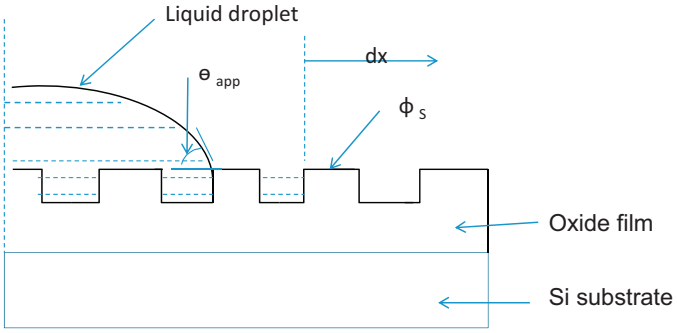

Fig. 6. Modelisation of the surface roughness of the composite film. The pore depth is ranging between 10 and 40 nm as indicated in Table 1.

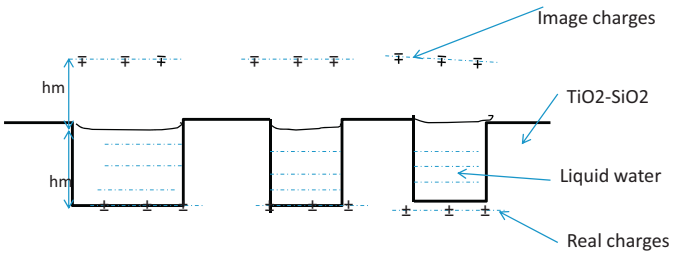

Fig. 7. Schematic representation of the electrochemical double layer and its electrostatic image.

The critical contact angle θ^0_{crit} evolves between $\theta^0_{crit} = 0$ which is obtained for a flat perfect surface ($r = 1$) and $\theta^0_{crit} = \pi/2$ which characterizes a completely porous solid obtained for large values of r.

3.2. Solid surface with an electrochemical double layer

In the case of a surface constituted by an oxide or a mixture of oxides, we have at the interface between the solid and the liquid (i.e. water or an ionic solution) the creation of an electrochemical double layer of thickness κ_D^{-1} (the Debye screening length).

The liquid/gas interface is characterized by a nearly vanishing electric field due to the great difference between the respective dielectric constant ($\varepsilon_{gas} = 1$ and $\varepsilon_{water} = 80$). So the double layer is repelled by an electrostatic image. This electrostatic repulsion was computed long ago by Langmuir [20].

The corresponding repulsive disjoining pressure gives rise to an electrostatic energy per unit area, G, corresponding to the electrostatic interaction between the real double layer and the image double layer as already proposed in [2,14].

Assuming a low surface potential of the solid, the electrostatic energy G per unit area can be written for monovalent ions in solution such as Na^+ and Cl^- [14].

$$G_{el.st} = \frac{2\sigma^2}{\varepsilon.\varepsilon_0}\frac{1}{\kappa_D}\ \exp -\kappa_D 2h \tag{6}$$

With σ the surface charge density, ε and ε_0 respectively the dielectric constant of the liquid and vacuum, 2 h is the distance between the two double layers as indicated in Fig. 7.

So, the variation of free energy of the prewetting film for a progression dx of the soaking front has to be corrected (neglecting the lateral edge electrostatic contribution):

$$dF = (\gamma_{SL} - \gamma_{SV})(r - \phi_S)dx + \gamma_{LV}(1 - \phi_S)dx + (1 - \phi_S)dxG_{el.st} \tag{7}$$

The condition of stability of the prewetting film ($dF \le 0$) with the Young equation gives the following new condition:

$$\cos\ \theta_E \ge \frac{1 - \phi_S}{r - \phi_S}\left(1 + \frac{G_{el.st}}{\gamma_{LV}}\right) = \cos\ \theta_{crit} \tag{8}$$

A new critical contact angle θ_{crit} is defined:

$$\cos\ \theta_{crit} = \cos\ \theta^0_{crit}.\left(1 + \frac{G_{el.st}}{\gamma_{LV}}\right)\ \text{with}\ \theta_E \le \theta_{crit}\ \theta^0_{crit} \tag{9}$$

The existence of the double layer is found to prevent the existence of a prewetting film. This result is consistent with the observation of de Gennes [2].

In reality we have to take into account the long range Van der Waals interactions which exist between the liquid/vapor interface and the solid/liquid interface so that the term $G_{el.st}$ has to be replaced by a term $G_{el.st} + G_{VdW}$ in the previous equations (neglecting the structural contribution which is the generally short range third interaction which complete the DLVO theory [14]).

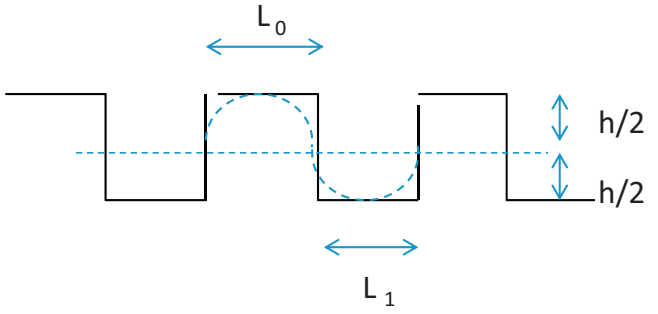

Fig. 8. Modeling of the surface roughness.

Following Israelachvili the Van der Waals contribution is written [14]:

$G_{VdW} = -A_{132}/12\pi h^2$ with A_{132} the non retarded Hamaker constant for media 1 and 2 interacting across medium 3.

Using the "combining relations" proposed in [14] we have:

$$A_{132} \approx (A_{11}^{1/2} - A_{33}^{1/2}) \cdot (A_{22}^{1/2} - A_{33}^{1/2})$$

For the experimental system we studied (a sol–gel TiO_2–SiO_2 film/water/air) we select in the reference book of Israelachvili [14].

$$A_{11} = A_{oxide} = \frac{1}{2}(A_{TiO_2} + A_{SiO_2}) = 24.6 \times 10^{-20}\ \text{J};$$

$$A_{33} = A_{water} = 3.7 \times 10^{-20}\ \text{J}$$

and $A_{22} = A_{air} = 0$ J, so we obtain $A_{132} = -5.8 \times 10^{-20}$ J

The Van der Waals contribution G_{VdW} is positive, but with typical values of h (between 10 nm and 70 nm) the numerical value of G_{VdW} is negligible ($G_{VdW} \approx 10^{-3}\ G_{el.st}$).

So in a first approximation Eq. (9) is consistent.

3.3. Evaluation of the critical contact angles and surface charge density

The first point in this evaluation (Eq. (9)) is the calculation of the contact angle θ^0_{crit} which is possible with our oversimplified representation of the surface roughness (Fig. 8)

The coefficient r takes a simplified form $r = L_0 + L_1 + 2h/L_0 + L_1 = 1 + 2h/L_0 + L_1$ with a surface fraction.

$$\phi_S = \frac{L_0}{L_0 + L_1}\quad \text{and}\quad \cos\ \theta^0_{cri} = \frac{1 - \phi_S}{r - \phi_S} = \frac{1}{1 + 2h/L_1} \tag{10}$$

In addition we have to take into account the cohesion of the liquid film so that:

$G_{el.st}(2h) \le 2 \cdot \gamma_{LV}$ so the various critical angles can be calculated depending on the values of the ratio $2\,h/L_1$ and taking the ratio $G_{el.st}/\gamma_{LV}$ as a parameter in Eq. (9).

As deduced from Table 2, knowing that the condition $\theta_E < \theta_{crit}$ must be fulfilled, reasonable values of θ_{crit} are obtained for $G_{el.st}/\gamma_{LV}$ close to 0.6–0.7 and for values of $2h/L_1$ close to 1.

With this assumptions Eq. (6) is written:

$$G_{el.st} = \frac{2\sigma^2}{\varepsilon\varepsilon_0}\kappa_D^{-1}\ \exp -2h\kappa_D = 0.7 \cdot \gamma_{LV} \tag{11}$$

It becomes possible to evaluate the surface charge density for limiting values of h for example in the case of typical NaCl concentrations.

The Debye screening length of an aqueous solution, at 25 °C for a 1:1 electrolyte e.g. NaCl is given by the following formula [14] obtained with $\varepsilon = 80$ and $\varepsilon_0 = 8.854.10^{-12}\ C^2\,J^{-1}\,m^{-1}$: $\kappa_D^{-1} =$

Table 2
Critical angles calculated for different values of the ratio $2h/L_1$ with the ratio $G_{el.st}/\gamma_{LV}$ as a parameter.

$2h/L_1$	$\cos\theta^0_{crit}$	θ^0_{crit} (°)	$\cos\theta_{crit}$	θ_{crit} (°)
$G_{el.st}/\gamma_{LV} = 0.6$				
0.8	0.555	56	0.88	27
0.9	0.526	58	0.84	33
1	0.500	60	0.80	37
1.8	0.357	69	0.57	55
$G_{el.st}/\gamma_{LV} = 0.7$				
0.8	0.555	56	0.943	19
0.9	0.526	58	0.894	26
1	0.500	60	0.850	32
1.8	0.357	69	0.607	53
$G_{el.st}/\gamma_{LV} = 0.9$				
0.8	0.555	56	1.05?	?
0.9	0.526	58	0.999	2
1	0.500	60	0.95	18
1.8	0.357	69	0.68	47

0.304 $(|\mathrm{NaCl}|)^{-1/2}$ nm. The values of σ calculated from Eq. (11) are given in Table 3.

Results given in Table 3 indicate reasonable values of surface charge density σ ranging between 1 μC/cm² and 5 μC/cm² in agreement with experimental values measured by AFM on SiO_2 and TiO_2–SiO_2 samples [16]. The high value of σ obtained for $h = 100$ nm and $\kappa_D^{-1} = 30.4$ nm is suspect due to the validity limit of Eq. (6) (low surface potential and low surface charge approximation).

A partial conclusion can be deduced from this preliminary theoretical analysis.

As proposed by Eq. (3) an apparent contact angle θ_{app} close to 0–5° can be obtained for low values of θ_E and low values of ϕ_S. In the case of a liquid/solid interface with an electrochemical double layer we can calculate a critical contact angle θ_{crit} with the condition $\theta_E \leq \theta_{crit}$.

Low but positive values of θ_{crit} are obtained for electro static interactions $G_{el.st} \leq \gamma_{LV}$ and aspect ratio of the surface roughness $2h/L_1$ close to 1. In this case, a reasonable surface charge density can be calculated (1–5 μC/cm²).

3.4. Stability of the prewetting film

In this paragraph we want to evaluate the variation of the free energy per unit area of the prewetting film with the thickness h.

Using Eq. (6) of the electrostatic energy $G_{el.st}$ which is the only term of the specific free energy of the film varying with the thickness h, we obtain:

$$dF = dG_{el.st} = \frac{-4\sigma^2}{\varepsilon.\varepsilon_0} \exp(-2\kappa_D h)\, dh \tag{12}$$

We observe the net tendency of the film to thicken ($dF < 0$ with $dh > 0$).

- A first consequence is an easy filling of the surface pore which exhibits a local equilibrium pressure P_r given by the Kelvin equation [15] (in a standard situation when the liquid wets the lateral face of the pore).

Table 3
Calculated surface charge density deduced from Eq. (11) for aqueous solutions with typical salt concentrations.

$\mathrm{NaCl} = 10^{-6}$ M/L, $\kappa_D^{-1} = 304$ nm			
h (nm)	10	50	100
σ (C/m²)	0.8×10^{-2}	0.9×10^{-2}	1.1×10^{-2}
$\mathrm{NaCl} = 10^{-4}$ M/L, $\kappa_D^{-1} = 30.4$ nm			
h (nm)	10	50	100
σ (C/m²)	3.4×10^{-2}	12.6×10^{-2}	64×10^{-2}

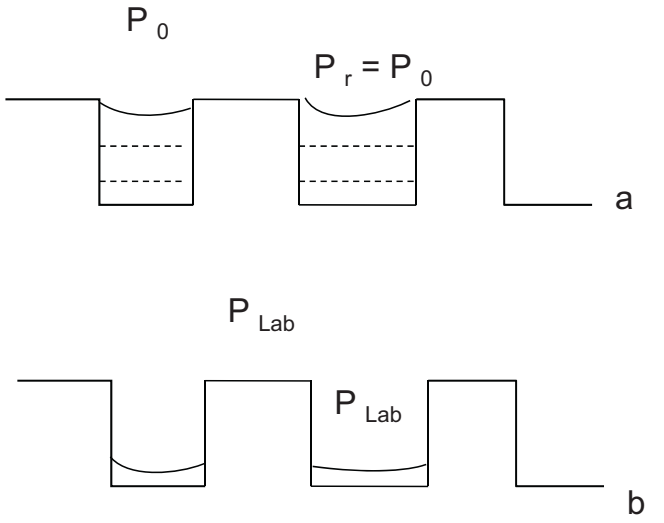

Fig. 9. Comparison between two situation: (a) the pore is completely filled under the equilibrium pressure P_0 and (b) the pore is partially empty under an imposed pressure P_{Lab}.

$$\frac{2\gamma_{LV}}{r_m} = -\frac{RT}{v_L} \ln\frac{P_r}{P_0} \tag{13}$$

with r_m the average radius of the pore, v_L the molar volume of the liquid, P_r and P_0 respectively the local partial pressure (inside the pore) and the external partial pressure of the water vapor near the liquid drop.

So is it reasonable to assume a complete filling of pores at the surface of our sample when studying an equilibrium situation as indicated in Fig. 6, with $P_r = P_0$

- A second consequence is the capacity of the liquid film to withstand to vaporization in a dry atmosphere. This capacity can be quantified:

As indicated in Fig. 9 the chemical potential of a mole of vapor can be expressed in the two situations:

In situation a: $\mu_{vap} = \mu_0 + RT \ln\left(\frac{P_r}{P_0}\right) = \mu_0$ when the pore is completely filled.

In situation b: $\mu_{vap} = \mu_0 + RT \ln\left(\frac{P_{Lab}}{P_0}\right)$ when the fixed external pressure is P_{Lab} (in absence of any liquid drops).

So between the two situations we have a variation of chemical potential:

$$\Delta_a^b\mu = RT \ln\frac{P_{Lab}}{P_0}$$

For a negative variation dh of the film thickness, the number of moles per unit area loosed by the film is

$\eta = \frac{1}{v_{Liq}} dh$ so that $\eta\Delta_a^b\mu = \frac{RT}{v_{Liq}} \ln\frac{P_{Lab}}{P_0} dh$

The variation of the free energy of the film taking into account a limited vaporization can be written:

$$dF = \left\{ \frac{-4\sigma^2}{\varepsilon.\varepsilon_0} \exp(-2\kappa_D h) - \frac{RT}{v_{Liq}} \ln\frac{P_{Lab}}{P_0} \right\} dh$$
$$\text{or } dF = -\left[2\kappa_D G_{el.st}(2h) + \frac{RT}{v_{Liq}} \ln\frac{P_{Lab}}{P_0} \right] dh \tag{14}$$

In this simple calculation we have neglected the variation of Gibbs energy corresponding to the variation of state (liquid/vapor) assuming we are close to the equilibrium state with an near equal number of adsorption and vaporization events.

Table 4
Calculated values of the critical ratio P_{Lab}^{crit}/P_0 assuming different values of the depth of surface pores h, the surface charge density and salt concentrations.

$\sigma = 10\ \mu C/cm^2$, $h = 10$ nm			
[NaCl]	10^{-4}	10^{-6}	10^{-8}
P_{Lab}^{crit}/P_0	0.810	0.684	0.669
$\sigma = 5\ \mu C/cm^2$, $h = 10$ nm			
[NaCl]	10^{-4}	10^{-6}	10^{-8}
P_{Lab}^{crit}/P_0	0.949	0.909	0.904
$\sigma = 5\ \mu C/cm^2$, $h = 30$ nm			
[NaCl]	10^{-4}	10^{-6}	10^{-8}
P_{Lab}^{crit}/P_0	0.986	0.927	0.905
$\sigma = 2\ \mu C/cm^2$, $h = 70$ nm			
[NaCl]	10^{-4}	10^{-6}	10^{-8}
P_{Lab}^{crit}/P_0	1	0.989	0.985

Eq. (14) can be written in a more standard formulation:

$$\frac{dF}{dh} = \left\{ \frac{dG_{el.st}}{dh} - \frac{RT}{v_{Liq}} \ln \frac{P_{Lab}}{P_0} \right\}$$

At equilibrium and introducing the disjoining pressure of Derjagin [21] we obtain a classical formula as proposed by Bormashenko and Starov [22b,23]:

$$\Pi(h) = -\frac{dG_{el.st}}{dh} = \frac{RT}{v_{Liq}} \ln \frac{P_0}{P_{Lab}} \quad (15)$$

The term in brackets of Eq. (14) is composed of two terms. The first electrostatic term is positive and the second is negative in a situation of dry atmosphere ($P_{Lab} < P_0$).

The compensation between the two terms ($dF = 0$) is obtained for a critical value P_{Lab}^{crit} when:

$$2\kappa_D G_{el.st}(2h) = -\frac{RT}{v_{Liq}} \ln \frac{P_{Lab}^{crit}}{P_0} \quad (16)$$

In a situation with $P_{Lab}^{crit} < P_{Lab} < P_0$ the electrostatic term is dominant in Eq. (14) and $dF/dh < 0$ indicating that $dF > 0$ for $dh < 0$ the film withstand to evaporation.

The alternative situation with $P_{Lab} < P_{Lab}^{crit} < P_0$ is obtained for $dF/dh > 0$ which imply a vaporization of the film.

A simple quantification of this effect is possible using Eq. (16) and typical values of the surface charge density σ and reasonable values of h the average depth of the surface pores.

We used standard values for the other parameters: $T = 293$ K; $v_{Liq} = 1.75.10^{-5}$ m^3/mole; $R = 8.314$ J K^{-1}mol^{-1}.

We obtain the following results indicated in Table 4.

4. The apparent contact angle: estimation and consequences

Surface model we have used in the first part is over simplified. In particular we have assumed that the solid in front of the triple line is composed by a patchwork of liquid water (in the pores) and dry solid. This last approximation can be revisited assuming the existence of a very thin film of water on the dry solid as indicated in Fig. 10.

The surface tension of the thin water layer can be expressed by the following equation in agreement with de Gennes [1], Bormashenko and Starov [22b,23].

$$\gamma_{th.film} = \left(\frac{dF}{dA}\right)_V = \gamma_{LV} + \gamma_{SL} + G(h) + h\Pi(h). \quad (17)$$

With A the surface area and $\Pi(h) = -dG(h)/dh$ the disjoining pressure which includes three components: Van der Waals, electro static and structural in the general case [14]. The stability condition of the film is expressed by the relation [1]:

$$\frac{d^2G}{dh^2} = -\frac{d\Pi(h)}{dh} \geq 0$$

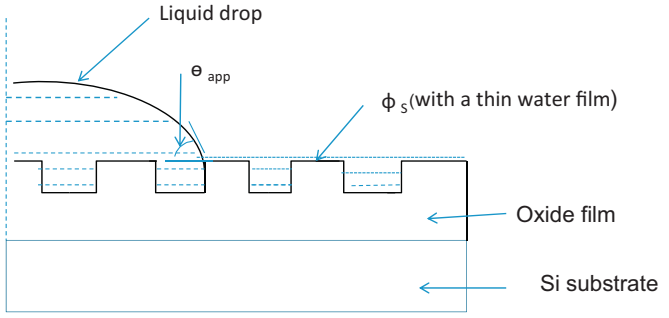

Fig. 10. Modelisation of the composite film assuming a patchwork of thin water layer and pores completely filled.

The situation we simulate as indicated in Fig. 10 corresponds to equilibrium between thin water layer and completely filled pores (equality of chemical potential). So the $G(h)$ energy can be represented as indicated in Fig. 11, with $G(h_2) = G_{el.st}(h_2) > 0$ avec $h_2 = h_{2max}$ the maximal depth of the pores and h_1.the thickness of the thin water film.

The common tangent between the point A and B indicates the identity of the chemical potential expressed by the relation

$$\Pi = \Pi(h_1) = \Pi(h_2) \quad (18)$$

In addition the identity of the surface tension between the thin water layer and the filled pore is written:

$$\gamma_{LV} + \gamma_{SL} + h_1\Pi(h_1) + G(h_1) = \gamma_{LV} + \gamma_{SL} + h_2\Pi(h_2) + G(h_2) \quad (19)$$

So, with $\Pi(h_1) = \Pi(h_2) = \Pi$, a discussion can be conducted in the case of a weak over saturation ($P_0/P_{Lab} \leq 1$) with, as indicated by Eq. (15),

$$\Pi = \frac{RT}{v_{liq}} \ln \frac{P_0}{P_{Lab}} \leq 0$$

$\Pi = G(h_1) - G(h_2)/h_2 - h_1 \leq 0$ this relation indicates $G(h_1) \leq G(h_2)$ with $G(h_2) = G_{el.st}(h_2) \succ 0$

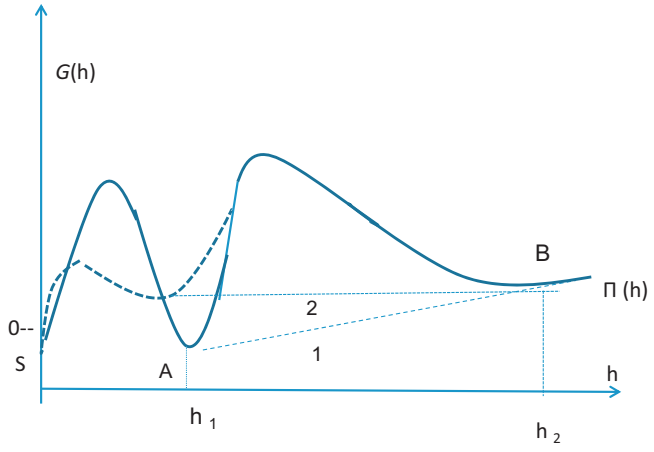

Fig. 11. Schematic representation of the specific interaction energy $G(h)$ versus h the thickness of the water layer corresponding to the simple model indicates in Fig. 10. The straight lines correspond to different situations: (1) $P_{Lab}/P_0 \geq 1$; (2) $P_{Lab}/P_0 = 1$, h_1 corresponds to the thickness of the thin water layer, h_2 is the depth of the filled pore.

The contact angle θ_{app} can be inserted by writing the equality of the surface forces at the level of the triple line

$$\gamma_{SL} + \gamma_{LV}\cos\theta_{app} = \gamma_{LV} + \gamma_{SL} + G(h_1) + h_1\Pi(h_1) = \gamma_{LV} + \gamma_{SL} + G(h_2) + h_2\Pi(h_2) \quad (20)$$

So:

$$\cos\theta_{app} - 1 = \frac{G(h_1)}{\gamma_{LV}} + h_1\frac{\Pi(h_1)}{\gamma_{LV}} \quad (21)$$

Assuming a weak value of $G(h_1)$ and the weak value h_1 of the thin water layer, we can obtain $\theta_{app} \approx 0$.

The spreading parameter S ($S = \gamma_{SV} - \gamma_{SL} - \gamma_{LV}$) is thus close to 0 as it can be deduced from the relation $\gamma_{LV}(\cos\theta_{app} - 1) = S$

In the case of a weak under saturation ($P_0/P_{Lab} \geq 1$) the disjoining pressure

$$\Pi = \frac{RT}{v_{liq}}\ln\frac{P_0}{P_{Lab}} \geq 0$$

The liquid drop is resting on a patchwork of solid film (fraction $1 - \phi_L$) and filled pores fraction (fraction ϕ_L).

The equilibrium of the surface forces at the level of the triple line is written:

$$\gamma_{LV}\cos\theta_{app} + \gamma_{SL} = \phi_L\left\{\gamma_{LV} + \gamma_{SL} + G(h_2) + h_2\Pi(h_2)\right\} + (1 - \phi_L)\gamma_{SV} \quad (22)$$

Eq. (22) can be modified using the relation $S = \gamma_{SV} - \gamma_{SL} - \gamma_{LV}$

$$\gamma_{LV}(\cos\theta_{app} - 1) = S(1 - \phi_L) + \phi_L\left\{G(h_2) + h_2\Pi(h_2)\right\} \quad (23)$$

A solution conducting to $\theta_{app} \approx 0$ is possible if S is negative taking into account the positive values of $G(h_2)$ and $\Pi(h_2)$.

An equation similar to Eq. (23) is obtained using the theorem of virtual works for a virtual displacement dx at the level of the triple line between the liquid drop and the patchwork of filled pore and solid island.

The theoretical discussion we have conducted in this last paragraph indicates that an apparent contact angle can be measured close to 0 assuming a spreading coefficient $S \leq 0$ in agreement with a low and positive equilibrium contact angle θ_E. This equilibrium contact angle should be close to the experimental value obtained under argon atmosphere (17–22°) and lower than the calculated critical angle θ_{crit} (Table 2).

In conclusion the experimental results obtained on the composite films can be understood. The stability of the quasi-filled surface pores under a weak under-saturation is able to explain the measured contact angles close to 0 during a long period of time. Due to the large fraction of surface pores, a protective contribution of this film can be understood despite a carbon contamination from the atmosphere during the aging.

This discussion remains schematic and would be improved by the introduction of a surface roughness at the level of solid islands.

5. Conclusions

The experimental results obtained on TiO_2–SiO_2 composite thin films via a sol–gel route confirm a natural and persistent superhydrophilicity. These properties can be easily photo-regenerated after a long aging period in ambient atmosphere.

The electrochemical double layer which classically exists between the oxides and aqueous solution is unfavorable to high wettability properties of ideal surfaces. Nevertheless taking into account the surface roughness and the electro-static contribution a reasonable surface charge density can be calculated in a qualitative agreement with the experimental values obtained on the composite TiO_2–SiO_2 films. In addition a stability study of the prewetting films indicates that this film is able to withstand to a weakly under saturated atmosphere.

Finally a theoretical analysis of the various water surface films indicates that a contact angle close to 0, as observed on the composite TiO_2–SiO_2 films, can be obtained for systems with spreading coefficient $S \leq 0$.

Our study which is very schematic can be improved in particular by a more realistic modeling of the surface rugosity. In particular it seems important to introduce two levels of surface roughness. The first level we have included can be completed by a roughness more limited at the level of solid islands.

The discussion dealing with the existence or not of a very thin water layer on the solid islands is schematic and can be improved by an in depth analysis including the different thickness of water at the level of drop, at the level of pore and at the level of very thin water layer including the effects of structural forces.

Nevertheless this study explains how the surface rugosity and the disjoining pressure caused by surface charges are able to explain the stability of a prewetting film which can withstand to vaporization.

This stability explains the persistence of the highly hydrophilic character of our composite surface films (TiO_2–SiO_2) with the exposition time to a standard atmosphere. It can be inferred that the prewetting water film has a protective function despite the carbon contamination induced by standard atmosphere.

Such a result can be applied to other systems. For example application to semi-conductor devices seems interesting. Similarly application in the field of corrosion tests of stainless steel seems promising. In particular the stability of thin water film containing a standard contaminant such as Cl^- ions can enhance corrosion degradation even in a dry atmosphere.

Acknowledgments

The financial support of these studies was provided by APERAM Company In the frame of grants with Grenoble Institute of Technology.

Scientific collaborations with Dr M.Langlet from the LMGP Laboratory of Grenoble Institute of Technology are particularly emphasized.

References

[1] P.G. de Gennes, F. Brochard-Wyart, D. Queré, Capillarity and Wetting Phenomenon, Springer, Berlin, 2003.
[2] P.G. de Gennes, Rev. Mod. Phys. 57 (3) (1985) 827.
[3] G. Whyman, E. Bormashenko, T. Stein, Chem. Phys. Lett. 450 (2008) 355–359.
[4] J. Bico, U. Thiele, D. Quéré, Colloids Surf. A Physicochem. Eng. Aspects 206 (2002) 41–46.
[5] V. Parry, G. Berthomé, J.-C. Joud, Appl. Surf. Sci. 258 (15) (2012) 5619.
[6] A. Shibuichi, T. Onda, N. Satoh, K. Tsujii, J. Phys. Chem. 100 (1996) 19512.
[7] E. Bormashenko, Y. Bormashenko, T. Stein, G. Whyman, J. Colloid Interface Sci. 311 (1) (2007) 212.
[8] J. Drelich, E. Chibowski, D. Desheng, K. Terpilowski, Soft Matter 7 (2011) 9804–9828.
[9] M. Houmard, D. Riasseto, F. Roussel, A. Bougeois, G. Berthome, J.-C. Joud, M. Langlet, Surf. Sci. 602 (21) (2008) 3364.
[10] M. Houmard, G. Berthome, J.-C. Joud, M. Langlet, Surf. Sci. 605 (3/4) (2011) 456.
[11] M. Langlet, A. Kim, M. Audier, C. Guillard, J.M. Hermann, J. Mater. Sci. 38 (2003) 3945.
[12] S. Permpoon, G. Berthome, B. Baroux, J.C. Joud, M. Langlet, J. Mater. Sci. 41 (22) (2006) 7650.
[13] M. Houmard, D. Riasseto, F. Roussel, A. Bourgeois, G. Berthome, J.-C. Joud, M. Langlet, Appl. Surf. Sci. 254 (2007) 1405.
[14] J. Israelachvili, Intermolecular and Surface Forces, second ed., Academic Press, San Diego, CA, 1991.

[15] A.W. Adamson, Physical Chemistry of Surfaces, 5th ed., J. Wiley & Sons, New York, 1990.
[16] M. Houmard, Grenoble Institute of Technology, 13 Mars, 2009 (PhD thesis).
[17] V.A. Parsegian, D. Gingel, Biophys. J. 12 (1972) 1192–1204.
[18] H.J. Butt, Biophys. J. 60 (1991) 777–785.
[19] A.B.D. Cassie, S. Baxter, Trans. Faraday Soc. 40 (1944) 546.
[20] I. Langmuir, J. Chem. Phys. 6 (1938) 893.
[21] B.V. Derjaguin, N.V. Churaev, J. Colloid Interface Sci. 49 (1974) 249.
[22] (a) E. Bormashenko, R. Progerb, T. Stein, Phys. Chem. Chem. Phys. 10 (2008) 4056–4061;
(b) E. Bormashenko, V. Starov, Colloid Polym. Sci. 291 (2013) 343–346.
[23] V.M. Starov, Adv. Colloid Interface Sci. 161 (2010) 139–152.